GENERATION AND ANALYSIS OF DIGITAL TWINS FOR CODICOFRP ACCOUNTING FOR FIBER LENGTH AND ORIENTATION DISTRIBUTION

Celine Lauff, Matti Schneider, and Thomas Böhlke*

Institute of Engineering Mechanics, Chair for Continuum Mechanics,
Karlsruhe Institute of Technology (KIT), Kaiserstraße 10, 76131 Karlsruhe,
Website: https://www.itm.kit.edu/cm
* Corresponding author (thomas.boehlke@kit.edu)

Keywords: Microstructure generation, Fiber-reinforced composites, Fiber orientation-length distribution

ABSTRACT

We present an adaption of the Orientation Corrected Shaking (OCS) method, originally developed for discontinuous short fiber-reinforced polymers, for generating continuous discontinuous fiber-reinforced polymers. Due to the combination of continuous and discontinuous reinforced phases, the interface between the two layers needs to be accounted for in a realistic way. The material flow during compression molding of CoDiCoFRP leads to ply migration at the interface resulting in an interlinked region between the layers, which is observable in 3D imaging. To account for this type of interface, we adapt the OCS method to enforce soft constraints for the fibers, i.e., a fiber's midpoint but not the entire fiber is constrained to its respective layer. Hence, at the interface fibers may penetrate the opposite phase, providing a link between the phases. In a computational study, we generate CoDiCoFRP with the OCS method and investigate whether the selection of the fiber length distribution type for given volume-weighted mean m and standard deviation s influences the effective stiffness of the generated microstructures. For Weibull, Gamma and log-normal distribution the results almost coincide, with differences smaller than 0.5%, revealing that for these cases the statistical quantities m and s are the only important descriptors to model the fiber length distribution.

1 GENERAL INTRODUCTION

Continuous discontinuous fiber-reinforced polymers (CoDiCoFRP) combine the advantages of their two constituents, i.e., the favorable stiffness to weight ratio of the continuously (Co) and the design freedom of the discontinuously (DiCo) reinforced phase. For this reason, CoDiCoFRP has a significant potential for lightweight applications.

Typical manufacturing processes lead to components whose local fiber microstructures are both random and highly anisotropic. As the effective properties depend on both the characteristics of the microstructure and the local constitutive properties, they are also anisotropic.

Computational homogenization methods [1] permit to reduce the high experimental effort to determine the mechanical properties of heterogeneous materials. To ensure reliable results, digital twins have to be generated which represent the real microstructures adequately. In this context, synthetic, i.e., generated, microstructures complement data obtained from 3D imaging, which is expensive to obtain in large numbers.

2 GEOMETRIC DESCRIPTION OF CODICOFRP

We consider a two-layer microstructure with rectangular cell $Q = [0, Q_1] \times [0, Q_2] \times [0, Q_3]$ in $\mathbb{R}^3$. The cell is filled with right circular cylindrical fibers in a non-overlapping configuration. The bottom layer with cell dimensions $Q_B = [0, Q_1] \times [0, Q_2] \times [0, Q_{IF}]$, where Q_{IF} denotes the height of the interface between the two layers, consists of N_B discontinuous fibers and the upper layer with cell dimension $Q_U = [0, Q_1] \times [0, Q_2] \times [Q_{IF}, Q_3]$ comprises N_U continuous and unidirectional fibers.

A fiber is described by its diameter D, its lengths L, its midpoint $\boldsymbol{x} \in Q$ and its direction $\boldsymbol{p} \in S^2$, where S^2 denotes the unit sphere in $\mathbb{R}^3$. The diameter D is assumed to be uniform for all fibers. For the

DiCo reinforced phase the fiber lengths follow a given fiber length distribution $\rho(L)$, i.e., are non-uniform. The fiber volume content is quantified by the fiber volume fraction, is computed in a non-overlapping configuration, e.g. for the bottom layer, via

$$\phi = \frac{\pi\, D^2}{4\, Q_1\, Q_2\, Q_{IF}} L_{\text{total}} \quad \text{with the total length} \quad L_{\text{total}} = \sum_{k=1}^{N_B} L_k\,. \tag{1}$$

For describing the fiber orientation, we use the fiber orientation tensors introduced by Advani et al. [2] and Kanatani [3] as a compact characteristic of the fiber orientation distribution. Considering N fibers with lengths L_k, the volume-weighted fiber orientation tensor of l^{th}-order computes as

$$\mathbb{A}_{<l>} = \frac{1}{L_{\text{total}}} \sum_{k=1}^{N} L_k\, \boldsymbol{p}_k{}^{\otimes l}. \tag{2}$$

For fiber reinforced composites, typically fiber orientation tensors of second order $\boldsymbol{A}$ are available. However, effective elastic properties are determined by the fiber orientation tensor of fourth order $\mathbb{A}$ [5]. To estimate fiber orientation tensors of higher order from fiber orientation tensors of second order, closure approximations are used [6]. For the Co reinforced phase, the fiber orientation tensor of second order is given as $\boldsymbol{A} \triangleq \text{diag}(1.0, 0.0, 0.0)$ in diagonal form due to the unidirectional arrangement of fibers in x-direction.

3 MICROSTRUCTURE GENERATION OF CODICOFRP

To generate microstructures of CoDiCoFRP which match the previously measured data accurately, the randomness of the fiber lengths and orientations needs to be considered. In contrast to pure DiCo material, the fiber's locations have to be constrained to their layer and the interfacial area between the layers has to be modelled. Additionally, we wish to ensure geometric periodicity of the generated volume elements, as this feature reduces the necessary size of the representative volume element [7] which in turn decreases the runtime of the microstructure generation and homogenization.

To attend to these tasks, we adapt the Orientation Corrected Shaking (OCS) method [8], which is capable of generating periodic microstructures for short fiber-reinforced polymers with almost planar fiber orientations. The OCS method accounts for a prescribed fiber length distribution, e.g., the Weibull-distribution, see Lauff et al. [8]. The fiber orientations are represented by an orientation tensor of fourth order, which is approximated from a prescribed fiber orientation tensor of second order by an intrinsic closure approximation.

To clarify the necessary adaptions of the OCS method, we briefly recall the general procedure of the algorithm first. In an initial step, fibers are sampled according to the prescribed fiber length distribution up to the necessary fiber volume fraction. For the initial configuration, the sampled fibers are placed in a planar and layer-wise unidirectional arrangement. With respect to the given second-order fiber orientation tensor in diagonal and ordered form

$$\boldsymbol{A} \triangleq \text{diag}(a_1, a_2, a_3) \quad \text{with} \quad a_1 \geq a_2 \geq a_3, \tag{3}$$

initial arrangement represents the fiber orientation tensor

$$\boldsymbol{A}_{\text{init}} \triangleq \text{diag}(a_1, a_2, 0) \,/\, (1\text{-}a_3) \tag{4}$$

exactly. Subsequent to the initial step, in the shaking step the fibers are shaken to introduce randomness. Starting with the longest fiber, for each fiber random changes of its midpoint and direction are made until a configuration is found where no collision with already shaken is detected. If such a configuration is not found within a maximum number of attempts m_{max}, then the microstructure generation will fail. For further details on the microstructure generation with the OCS method, see Lauff et al. [8].

To adapt the initial step for the microstructure generation of CoDiCoFRP, we conduct the initial procedure for each layer within its respective cell Q_U or Q_B separately. Afterwards, the two cells are joined together to obtain the entire cell Q.

For the shaking step, two modifications are necessary: First, we have to account for the interfacial region between the two layers. Due to the material flow during compression molding of CoDiCoFRP, ply migration between the two phases occurs [9]. To account for the linked interface, we model the

fibers' locations with soft constraints, i.e., the midpoints but not the entire fiber are constrained to the respective layer of the fiber. We realize the soft constraints within the OCS method by correcting the z-component of a fiber's midpoint if it has changed. The correction follows the prescription

$$x_z = \begin{cases} L_{\min}, & x_z < L_{\min}, \\ L_{\max}, & x_z > L_{\max}, \\ x_z, & otherwise, \end{cases} \tag{5}$$

where $L_{\min}$ denotes the lower boundary in z-direction of the fiber's layer and $L_{\max}$ the upper boundary. The second modification concerns the shaking order of the fibers to ensure that the typically high volume fraction in the Co reinforced phase is reached. Hence, first the Co fibers are shaken. Subsequently, the remaining DiCo fibers are shaken in descending order of their lengths.

In Figure 1, a synthetic microstructure of CoDiCoFRP generated with the adapted OCS method is shown. The edge length of the microstructure is $Q_i = 600\mu$m and the Co reinforced tape occupies one sixth of the total height. For both phases, the fiber diameter is $D = 10\mu m$. For the DiCo reinforced phase, the second-order fiber orientation tensor $\boldsymbol{A} \triangleq \mathrm{diag}(0.79, 0.19, 0.02)$ is prescribed and the fiber lengths are sampled from the Weibull distribution with volume-weighted mean $m = 250\mu$m and a standard deviation $s = 120\ \mu$m. The fiber volume fraction in the DiCo reinforced phase is 15% and in the Co reinforced phase 40%.

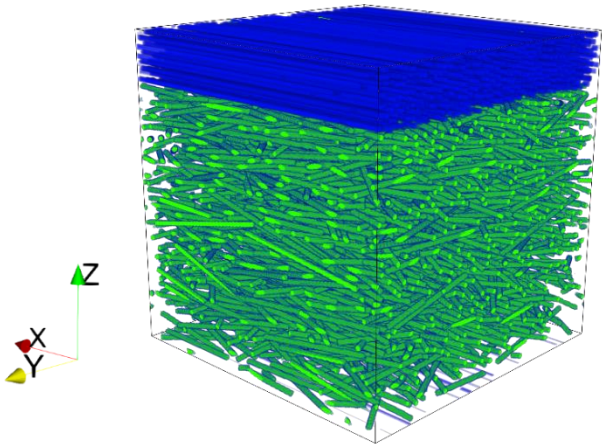

Figure 1: Synthetic microstructure for CoDiCoFRP generated with the adapted OCS method.

4 PROBABILITY DISTRIBUTIONS TO MODEL THE FIBER LENGTH DISTRIBUTION

As a result of the manufacturing process, the fiber lengths in the DiCo reinforced phase vary throughout the component. In engineering practice, typically the measured volume-weighted mean m and standard deviation s of real fiber-reinforced microstructures are available as elementary statistics of the fiber length distribution. According to Mehta and Schneider [10], sampling lengths from an adequate distribution function with respect to both the volume-weighted mean m and standard deviation s permits to capture the influence of varying fiber lengths on the effective properties, i.e., the assumption of constant lengths of mean m is not sufficient for generating representative volume elements. Due to the lack of knowledge on the underlying distribution function, the type of distribution to model the fiber length distribution needs to be chosen for the microstructure generation. For short-fiber reinforced composites, the Weibull distribution, defined via the density function

$$\rho_{\lambda,\beta}(L) = \frac{\beta}{\lambda}\left(\frac{L}{\lambda}\right)^{\beta-1} e^{-(L/\lambda)^{\beta}}, \quad L, \lambda, \beta > 0, \tag{6}$$

the Gamma distribution, defined via the density function

$$\rho_{\alpha,\beta}(L) = \frac{\beta^{\alpha}}{\Gamma(\alpha)} L^{\alpha-1} e^{-\beta L}, \quad \Gamma(z) = \int_0^{\infty} t^{z-1}\, e^{-t}\, \mathrm{d}t\,, \quad L, \alpha, \beta > 0 \tag{7}$$

and the log-normal distribution, defined via the density function

$$\rho_{\sigma_n,\mu_n}(L) = \frac{1}{\sigma_n\, L\, \sqrt{2\pi}}\, e^{-\frac{(\ln L - \mu_n)^2}{2{\sigma_n}^2}}, \quad L, \sigma_n, \mu_n > 0 \tag{8}$$

are typically used for modelling the fiber length distribution [11, 12, 13]. In Figure 2, the Weibull, Gamma and log-normal distribution functions with equal volume-weighted mean $m = 250\mu m$ and standard deviation $s = 120\ \mu$m are shown. All three distribution functions show a similar qualitative curve, which is characterized with a peak at fiber lengths shorter than the volume-weighted mean m and small probabilities for very long fibers. This overall behavior matches with the fiber length distributions measured for real short fiber-reinforced composites [4]. However, the distribution functions differ in the exact quantitative values, which in turn influence the realized fiber lengths in the generated microstructures.

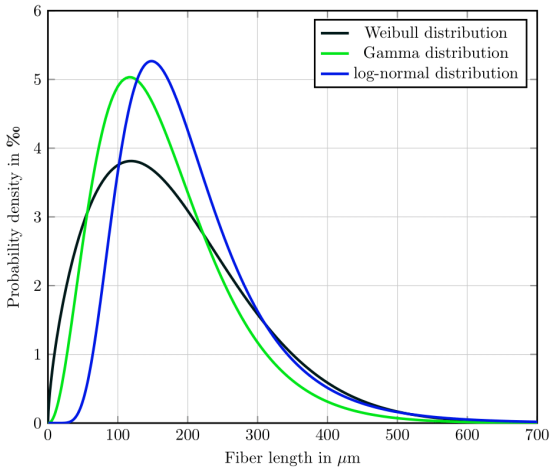

Figure 2: Weibull, Gamma and log-normal distribution with volume-weighted mean $m = 250\mu m$ and standard deviation $s = 120\ \mu$m.

5 COMPUTATIONAL INVESTIGATIONS

5.1 Setup

For the Co and the DiCo fiber-reinforced phase, we consider a PA66 matrix with E-glass fibers. The isotropic elastic parameters are listed in Table 1, obtained by Hessman et al. [11].

E-glass fibers	PA66 matrix
$E = 72.0$ GPa	$E = 3.0$ GPa
$\nu = 0.22$	$\nu = 0.40$

Table 1: Material properties for the PA66 matrix and the E-glass fibers [11].

We assume a fiber diameter of $D = 10\mu m$. For the DiCo reinforced phase, we prescribe a second-order fiber orientation tensor $\boldsymbol{A} \triangleq \mathrm{diag}(0.79, 0.19, 0.02)$ and as statistical quantities for the fiber length

distribution a volume-weighted mean $m = 250\mu\text{m}$ and a standard deviation $s = 120\ \mu\text{m}$. The fiber volume fraction in the DiCo reinforced phase is 15% and in the Co reinforced phase is 40%. We generate periodic microstructures with cubic cell-size with dimensions $Q_i = 600\mu\text{m}$, where the Co reinforced tape occupies one sixth of the total height.

Within the OCS method, we correct fiber directions until the relative error of fiber-orientation tensor of fourth order is lower than 10^{-4}. We choose as minimum fiber distance 20% of the fiber diameter, i.e., 2 μm. The selected shaking parameters as well as the maximum number of attempts for the OCS method are listed in Table 2.

α	β	$\Delta\varphi_2$	m_{max}
4	2	$3\pi/8$	10^7

Table 2: Used algorithmic parameters for the OCS method.

The effective elastic properties are computed with FFT-based computational homogenization software [14, 15], a discretization on a staggered grid [16] and a conjugate gradient solver [17, 18], terminated at a relative tolerance of 10^{-5}. We refer to the review article [19] for background. For the computation of the effective properties, the voxel edge-length is set to $2\mu\text{m}$. The effective elastic constants are computed based on six independent load cases. As the second-order fiber orientation tensor is orthotropic, also the effective properties are orthotropic on average. Hence, we report on the effective orthotropic engineering constants, which are approximated from the effective elastic tensor [20, 21].

5.2 Comparison of the effective stiffness for different fiber length distributions

An accurate realization of the elementary statistical quantities, both the volume-weighted mean m and the standard deviation s, of the fiber length distribution permits to generate microstructures with matching effective properties compared to experimental data [10]. In this section, we study whether besides the elementary statistical quantities also the selected fiber length distribution type has an influence on the effective stiffness of the synthetic microstructures. Therefore, we consider the Weibull, Gamma or log-normal distribution as fiber length distribution, which are typically used for short fiber-reinforced polymers in literature. For each distribution function, we generate ten microstructures and compute the effective stiffness. The mean values and the standard deviations of the approximated orthotropic Young's moduli are listed in Table 3.

	E_1 GPa	E_2 GPa	E_3 GPa	err_{orth} %
Weibull	11.44 $\pm$ 0.03	5.33 $\pm$ 0.01	4.96 $\pm$ 0.01	0.57 $\pm$ 0.01
Gamma	11.48 $\pm$ 0.03	5.34 $\pm$ 0.01	4.96 $\pm$ 0.01	0.57 $\pm$ 0.01
log-normal	11.45 $\pm$ 0.02	5.33 $\pm$ 0.01	4.96 $\pm$ 0.00	0.59 $\pm$ 0.02

Table 3: Comparison of the approximated effective Young's moduli of microstructures generated with the Weibull, Gamma or log-normal distribution function as fiber length distribution with volume-weighted mean $m = 250\mu\text{m}$ and standard deviation $s = 120\ \mu\text{m}$.

As we report on the effective orthotropic engineering constants, we need to control the quality of the orthotropic approximation of the effective elastic tensor. By assessing the orthotropic approximation error $\mathrm{err}_{\mathrm{orth}}$, we observe small errors below 1% confirming that the orthotropic approximation of the measured effective stiffness is suitable.

Let us focus on the approximated orthotropic Young's moduli. The results feature small random errors, which confirms the representativity of the chosen unit cell size. We observe that the results almost coincide for all fiber length distribution functions. The highest relative difference of 0.35% is computed for the Young's modulus E_1 between the Weibull and log-normal distribution. Hence, it appears that the selection of one of those three distribution functions has no significant influence on the computed effective stiffness. As a result of this study, we emphasize that the volume-weighted mean m and the standard deviation s are sufficient descriptors for the fiber length distribution of short fiber-reinforced composites when combined with a fiber length distribution following the overall behavior shown in Figure 2.

6 CONCLUSIONS

In this work, we presented an adaption of the Orientation Corrected Shaking (OCS) method [8] to generate CoDiCoFRP consisting of a discontinuously reinforced bottom layer and a continuously reinforced upper layer. Therefore, we enabled the assembly of several cells to an entire microstructure for the initial step of the OCS method. Within the shaking step, we implemented soft constraints in the form of a correction of the fibers' midpoints to force them to be in their respective layer. By using these soft constraints, we realized a linking between the Co and the DiCo reinforced phase, which is typically observed for real CoDiCoFRP. Additionally, the shaking order of the fibers is changed, i.e., the Co reinforced fibers are shaken first and subsequently the DiCo reinforced fibers are shaken in descending order of their lengths, to ensure the capability of achieving high volume fractions in the Co reinforced phase.

The work includes a study whether the selection of the fiber length distribution type for given volume-weighted mean and standard deviation influences the effective stiffness of the generated microstructures. We observed that the results almost coincide for all fiber length distribution functions, with differences smaller than 0.5%. Hence, we conclude that the distribution function has no significant influence on the effective stiffness as long as the overall behavior of the distribution function follows the quantitative shape shown in Figure 2. We emphasize that the important quantities to describe the fiber length distribution are the volume-weighted mean and standard deviation.

ACKNOWLEDGEMENTS

The research documented in this manuscript has been funded by the German Research Foundation (DFG), project number 255730231, within the International Research Training Group "Integrated engineering of continuous-discontinuous long fiber reinforced polymer structures" (GRK 2078). The support by the German Research Foundation (DFG) is gratefully acknowledged.

REFERENCES

[1] K. Matouš, M. G. D. Geers, V. G. Kouznetsova und A. Gillman, A review of predictive nonlinear theories for multiscale modeling of heterogeneous materials, *Journal of Computational Physics*, 330, 2017, pp. 192–220.

[2] S. G. Advani und I. I. I. C. L. Tucker, The Use of Tensors to Describe and Predict Fiber Orientation in Short Fiber Composites, *Journal of Rheology,* **31**, 1987, pp. 751–784.

[3] K.-I. Kanatani, Distribution of directional data and fabric tensors, *International Journal of Engineering Science*, **22**, 1984, pp. 149–16.

[4] P. A. Hessman, T. Riedel, F. Welschinger, K. Hornberger und T. Böhlke, Microstructural analysis of short glass fiber reinforced thermoplastics based on x-ray micro-computed tomography, *Composites Science and Technology,* **183**, 2019, pp. 107752.

[5] V. Müller, M. Kabel, H. Andrä und T. Böhlke, Homogenization of linear elastic properties of short-fiber reinforced composites – A comparison of mean field and voxel-based methods, *International Journal of Solids and Structures,* **67–68**, 2015, pp. 56–70.

[6] S. K. Kugler, A. Kech, C. Cruz und T. Osswald, Fiber Orientation Predictions - A Review of Existing Models, *Journal of Composites Science,* **4**, 2020, pp. 69.

[7] M. Schneider, M. Josien und F. Otto, Representative volume elements for matrix-inclusion composites - a computational study on the effects of an improper treatment of particles intersecting the boundary and the benefits of periodizing the ensemble, *Journal of the Mechanics and Physics of Solids,* **158**, 2022, pp. 104652.

[8] C. Lauff, M. Schneider, J. Montesano und T. Böhlke, An orientation corrected shaking method for the microstructure generation of short fiber-reinforced composites with almost planar fiber orientation, **Submitted**, 2023, pp. 1-21.

[9] D. Corbridge, L. Harper und N. W. D.S.A. De Focatiis, Compression moulding of composites with hybrid fibre architectures, *Composites: Part A,* **95**, 2017, pp. 87-99.

[10] A. Mehta und M. Schneider, A sequential addition and migration method for generating microstructures of short fibers with prescribed length distribution, *Computational Mechanics,* **70**, 2022, pp. 829–851.

[11] P. A. Hessman, F. Welschinger, K. Hornberger und T. Böhlke, On mean field homogenization schemes for short fiber reinforced composites: Unified formulation, application and benchmark, *International Journal of Solids and Structures,* **230-231**, 2021, pp. 111141.

[12] Z. Li, Z. Liu, Y. Xue und P. Zhu, A novel algorithm for significantly increasing the fiber volume fraction in the reconstruction model with large fiber aspect ratio, *Journal of Industrial Textiles,* **51**, 2022, pp. 506–530.

[13] H. Shen, S. Nutt und D. Hull, Direct observation and measurement of fiber architecture in short fiber-polymer composite foam through micro-CT imaging *Composites Science and Technology,* **64**, 2004, pp. 2113–2120.

[14] K. Breuer und M. Stommel, RVE modelling of short fiber reinforced thermoplastics with discrete fiber orientation and fiber length distribution, *SN Applied Sciences,* **2**, 2019, pp. 91.

[15] H. Moulinec und P. Suquet, A numerical method for computing the overall response of nonlinear composites with complex microstructure, *Computer Methods in Appled Mechanics and Engineering,* **157**, 1998, pp. 69–94.

[16] M. Schneider, F. Ospald und M. Kabel, Computational homogenization of elasticity in a staggered grid *International Journal for Numerical Methods in Engineering,* **105**, 2016, pp. 693–720.

[17] J. Zeman, J. Vondřejc, J. Novak und I. Marek, Accelerating a FFT-based solver for numerical homogenization of periodic media by conjugate gradients, *Journal of Computational Physics,* **229**, 2010, pp. 8065–8071.

[18] S. Brisard und L. Dormieux, Combining Galerkin approximation techniques with the principle of Hashin and Shtrikman to derive a new FFT-based numerical method for the homogenization of composites *Computer Methods in Applied Mechanics and Engineering,* **217–220**, 2012, pp. 197–212.

[19] M. Schneider, A review of non-linear FFT-based computational homogenization methods, *Acta Mechanica,* **232**, 2021, pp. 2051–2100.

[20] J. Görthofer, M. Schneider, F. Ospald, A. Hrymak und T. Böhlke, Computational homogenization of sheet molding compound composites based on high fidelity representative volume elements, *Computational Materials Science,* **174**, 2020, pp. 109456.

[21] S. C. Cowin, The relationship between the elasticitiy tensor and the fabric tensor *Mechanics of Materials,* **4**, 1985, pp. 137–147.